Rapid Communications | Editors' Suggestion

Compression-induced resistance of singlet oxygen dissociation on phosphorene

Lance Kavalsky [1], Sankha Mukherjee [1], and Chandra Veer Singh [1,2,*]

[1] *Department of Materials Science and Engineering, University of Toronto, 184 College Street, Suite 140, Toronto, Ontario, Canada M5S 3E4*

[2] *Department of Mechanical and Industrial Engineering, University of Toronto, 5 King's College Road, Toronto, Ontario, Canada M5S 3G8*

(Received 30 October 2019; accepted 22 January 2020; published 24 February 2020)

Phosphorene is a promising two-dimensional material for electronics, energy, and catalysis applications, but its instability in ambient conditions is a major obstacle in its commercialization. The degradation begins with dissociation of O_2 onto the surface of phosphorene which is spontaneous in its singlet state. Focusing on singlet O_2 splitting, compressive strain is proposed as a method of inducing an activation barrier to this process. Applying compressive strain introduced a barrier as large as 0.45 eV causing a decrease in the rate constant by seven orders of magnitude. Introducing entropic effects via metadynamics biased *ab initio* molecular dynamics allowed for the generation of free-energy landscapes. Through this method, the largest barrier was observed to be 0.33 ± 0.04 eV causing a decrease in the kinetic rate constant by five orders of magnitude. These results highlight compression as a method of inhibiting singlet oxidation of phosphorene and pave the way towards further experimental investigation.

DOI: 10.1103/PhysRevMaterials.4.021001

Phosphorene is a novel two-dimensional (2D) material analogous to graphene which has shown potential for areas such as energy storage [1–4], photocatalysis [5], and electronics [6]. For example, it has shown some of the highest specific capacities to date as a composite anode in Na-ion batteries [7], and few-layer flakes were also able to help limit the shuttle effect in Li-S batteries [8]. From these demonstrated successes, phosphorene holds much promise to carry energy technologies forward.

Despite this material's promise, degradation in ambient conditions containing light, oxygen, and humidity has been an obstacle preventing phosphorene from widespread implementation [1,2,6,9–11]. This process involves the bubbling and collapse of the material and can severely hinder performance as mobility decreases rapidly over exposure time [12,13]. It is widely agreed upon that degradation begins with excited O_2 splitting on phosphorene [14]. Studies into the dissociation mechanism of O_2 onto phosphorene theorize that after making a triplet-to-singlet transition, singlet O_2 can spontaneously split on the surface of phosphorene [15]. The triplet state is the ground state where the two electrons in the π^* orbitals are aligned, whereas the singlet state is an excited state where they are antialigned [15]. With the goal of using phosphorene for applications in open-air conditions, this ambient stability requires further investigation. Thicker samples show slowed degradation as the band gap closes [14], but this also can hamper catalytic performance, and fewer layers can make easier access for molecules to the active sites. Much work has been conducted to explore methods of increased stability by prohibiting oxygen from reacting with the phosphorene substrate including doping and encapsulation [16–18]. In addition to these approaches, it was shown that heat treatments could increase stability of few-layer black phosphorus in the presence of reactive oxygen species (e.g., singlet O_2), possibly due to removal of intercalated H_2O [19]. However, these approaches have limited applicability as encapsulation or doping restricts interaction with O_2 which may be necessary in some applications (e.g., Li-air batteries), and increasing the temperature is not a viable option in all applications (e.g., batteries, in general).

Studies into metal surfaces and silicene (two-dimensional form of silicon) have highlighted strain engineering as an avenue for tuning electronic and catalytic properties through both theoretical and experimental methods [20–24]. Numerous methods have been explored for which strain has been successfully applied to 2D materials including bending of a flexible substrate, deposition on a substrate to induce wrinkling, and thermal mismatch between materials [25,26]. Additionally, lattice mismatch can yield strain, and, in the context of phosphorene, there is a rising number of growth methods on different substrates including Si/SiO_2, polymers, and polyester [27,28]. Recently, a top-down method has been put forward which can yield phosphorene nanoribbons up to 0.075 mm in length [29]. Moreover, phosphorene's electronic properties have been shown theoretically to be receptive to applied strains [30], and a recent density functional theory (DFT) study investigated the role of applied strain with respect to a lone O atom [31]. Experimentally uniaxial strain has been applied to phosphorene through controlled wrinkling on a gel film [32,33]. Also, phosphorene on a $MoSe_2$ substrate has been studied computationally to show increased resistance [34]. However, it remains unclear whether specifically strain engineering can be utilized to inhibit the O_2 dissociation process.

In this Rapid Communication, we propose lattice compression as an approach towards significantly inhibiting singlet O_2 dissociation on phosphorene. We found that, at the ground state, different methods of compression could induce barriers towards singlet O_2 splitting and used crystal orbital Hamilton

*Corresponding author. chandraveer.singh@utoronto.ca

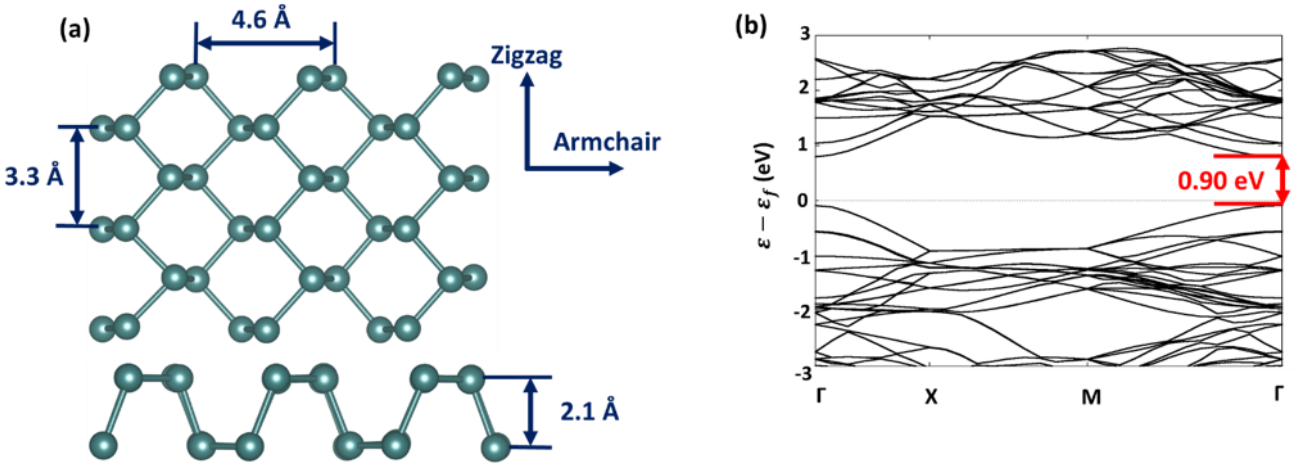

FIG. 1. (a) Geometric properties of relaxed phosphorene. Each of the lattice parameters is given, and the zigzag and armchair directions are defined and (b) electronic structure of bare relaxed phosphorene. The direct band gap at Γ is highlighted with red arrows.

population (COHP) analysis [35–37] to further study the mechanisms. Introduction of thermal effects into the simulations showed that compression via either applied strain or thermal mismatch could also induce free-energy barriers to the dissociation process.

Phosphorene's structure gives it two in-plane anisotropic symmetry axes: zigzag and armchair (Fig. S1a of the Supplemental Material [38]). All systems were simulated from a first-principles density functional theory approach using QUANTUM ESPRESSO [39]. In order to avoid spin contamination (where the spin states are no longer eigenfunctions of the total spin operator), singlet oxygen was modeled using non-spin-polarized DFT as performed elsewhere [15]. Singlet oxygen is the excited state of O_2 due to Hund's rule and, thus, is in a higher-energy state than the spin-aligned triplet state. Dissociation on lattices under uniaxial, biaxial, and equibiaxial compressions were simulated using the nudged elastic band method which gives the minimum energy pathway at the ground state. This gives an estimate towards activation barriers neglecting any thermal effects, such as entropy. Further studying the electronic stability of these structures, COHP analysis was used through the LOBSTER [40] package. To introduce thermal effects, such as entropy and zero-point energy, metadynamics biased *ab initio* molecular dynamics (AIMD) was used through PLUMED [41] and QUANTUM ESPRESSO [39] thereby giving free-energy barrier predictions. Additional computational details are provided in the Supplemental Material [38].

Relaxed phosphorene was found to be a direct band-gap semiconductor with a band gap of 0.90 eV (Fig. 1). Our lattice parameters of 3.3 and 4.6 Å were found to be comparable to reported literature values of 3.35 and 4.62 Å [42] and 3.298 and 4.627 Å [30]. Moreover, our band gap was found to be in agreement with previous results which reported gaps of 1 eV [42], 0.8 eV [43], and 0.91 eV [30]. The electronic structure and band gap are highly dependent upon the choice of exchange correlation. Although advanced functionals, such as hybrid functionals, can yield band gaps closer to experimental results, they are significantly more computationally expensive. As we are concerned with differences in energy, we employ the Perdew-Burke-Ernzerhof exchange-correlation functional [44]. Fixing the armchair direction while applying compression in the zigzag direction, conversely fixing the zigzag direction, and compressing the armchair direction, both saw a decreasing band gap [Fig. 2(a)] as seen elsewhere [30]. Since compression is observed to influence the electronic properties of the system, the question arises of how this will present itself in catalysis scenarios. Relaxed phosphorene (0% strain) was able to dissociate singlet oxygen spontaneously onto the phosphorene surface with the charge-density difference shown in Fig. 2(b). Through the charge-density difference, it is shown that each O atom will pull charge from the lattice as oxygen is more electronegative than phosphorus. It is also observed that the O_2 bond expands from 1.22 to 2.78 Å corresponding to a 128% increase. This unstrained scenario represents a baseline for all subsequent landscapes and means that any barrier introduced is an improvement in terms of oxidation resistance. When introducing strain uniaxially in the zigzag direction, no activation barrier towards splitting was observed in the studied range where a barrier of 0.30 eV was found at 1% strain in the armchair direction. Energy profiles and activation barrier trends as a function of strain are given in Figs. S1a–S1c of the Supplemental Material [38]. The dissimilar behavior between these two conditions can be explained by different Poisson ratios in phosphorene for each axis which results in different magnitudes of lateral expansion. However, it is important to note that these uniaxial scenarios allow free lateral expansion.

We next applied compression with the lateral direction held fixed, which is analogous to biaxial loading owing to Poisson's contraction. Interestingly, compressing the armchair direction with the zigzag dimension pinned shows similar behavior to that of the uniaxial armchair strain with a maximum barrier of 0.38 eV (Figs. S1d and S1e of the Supplemental Material [38]). However, the opposite scenario induced activation barriers for a larger range of strains with emergence of a physisorbed state starting at 1% [Fig. 2(c)] with the barrier reaching as high as 0.45 eV [Fig. 1(d)]. To summarize, for strain applied in this manner, if the magnitude of compression is larger than the threshold of 1%, then the oxidation process will be slowed. The reader may note that the final energetic state appears to be independent of strain in Fig. 1(c). This

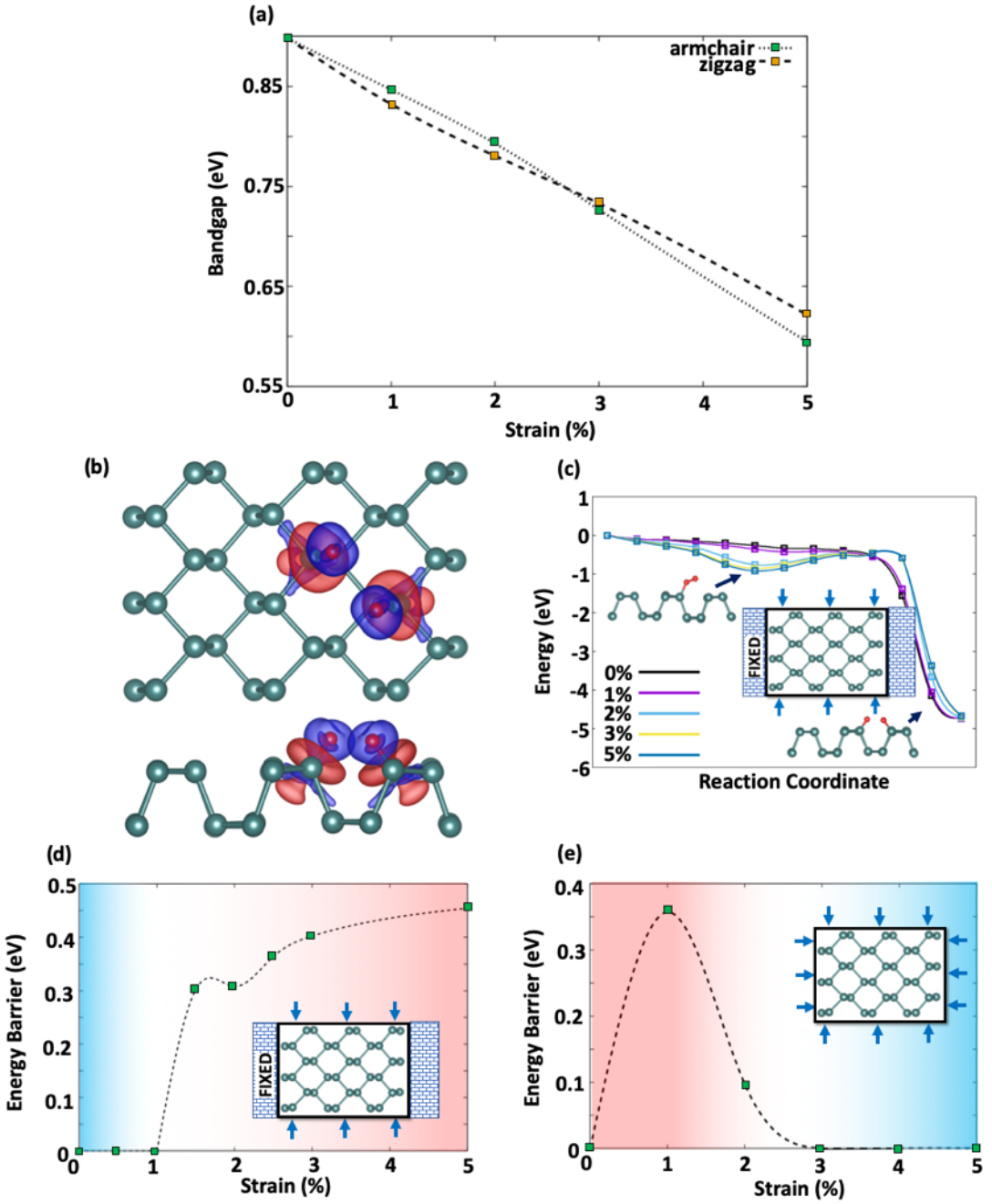

FIG. 2. (a) Band-gap variation of phosphorene under strains in each direction with the lateral direction fixed. (b) Charge-density difference (isosurface set to 0.0036 $e\text{Å}^{-3}$) of dissociated O_2 on phosphorene. Color code: purple = charge accumulation, red = charge depletion; (c) energy profiles for strains applied in the zigzag direction with the armchair dimension pinned; energy barriers as a function of strain are plotted for (d) fixed armchair dimension and zigzag compression and (e) fixed zigzag dimension and armchair compression.

can be explained through the initial reference state also being a function of the applied strain. Moreover, this quantity is essentially an adsorption energy which has been shown previously to have a strain dependence of order 0.1 eV in other systems [20–22]. In addition to the uniaxial type compression, equibiaxial strain was applied to the system with the energy barriers shown in Fig. 2(e). A window of barriers emerges reaching as high as 0.36 eV. Profiles corresponding to this type of applied strain are shown in Fig. S1f of the Supplemental Material [38]. The behavior seen here is almost identical to armchair compression with and without pinned lateral dimensions. Therefore, for applying equibiaxial strain, oxidation can be slowed via compression of phosphorene if applied in the appropriate regime. To summarize, compression can lead to induced oxidation resistance at the ground state with an overall maximum barrier of 0.45 eV. To place this result in the context of the relaxed state, the Arrhenius equation can be used

$$k = k_0 \exp\left(\frac{-E_A}{k_B T}\right),$$

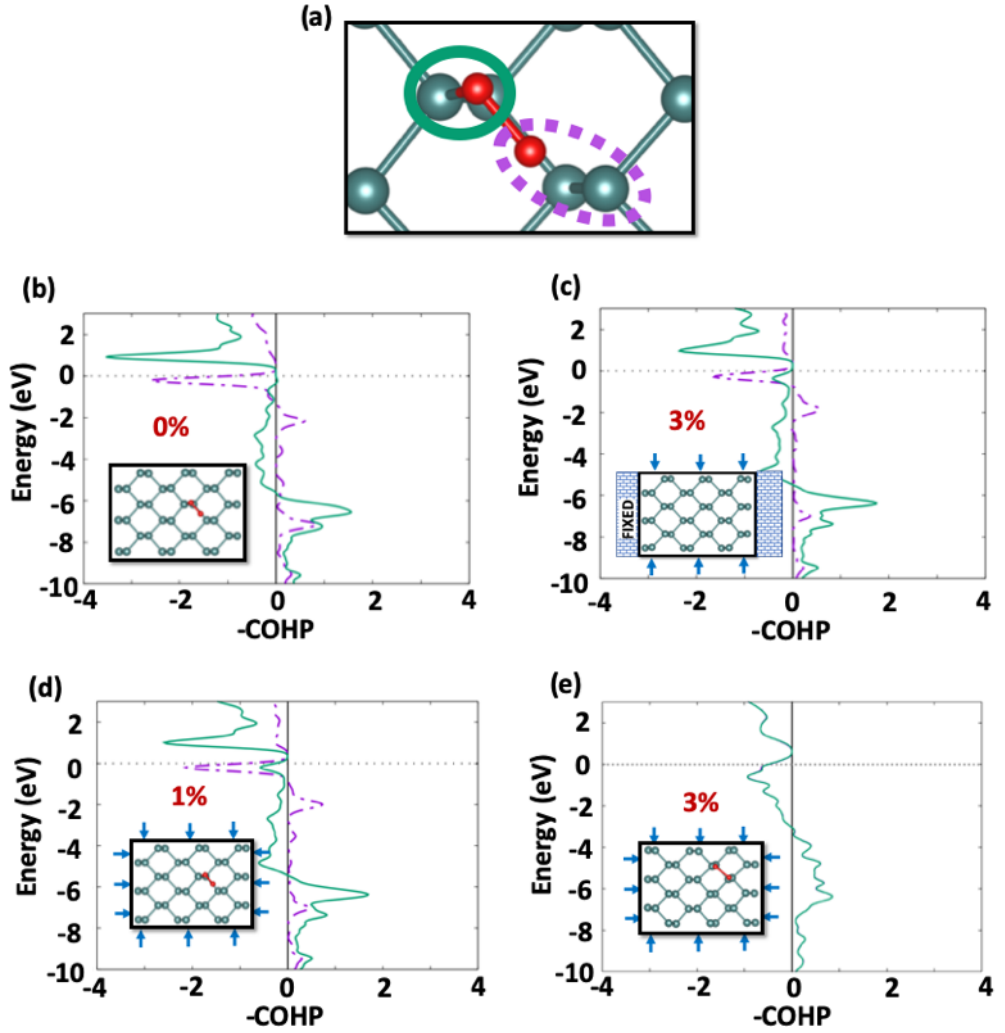

FIG. 3. COHP analysis was conducted for both P-O pairs to evaluate electronic instability of the transition states at varying compressions. Antibonding states at the Fermi level indicates electronic instability. $+ve$ is bonding and $-ve$ is antibonding. (a) Illustration highlighting the P-O interactions considered for COHP analysis. COHP profiles for (b) relaxed system, (c) 3% compression along the zigzag direction with lateral pinning, (d) 1% equibiaxial compression, and (e) 3% equibiaxial compression.

where k is the kinetic rate constant, k_0 is a prefactor, E_A is the activation barrier, T is the temperature, and k_B is the Boltzmann constant. Extrapolating the barrier to 300 K, the kinetic rate constant will decrease by up to seven orders of magnitude, significantly slowing the process.

To understand the different observed trends of induced barrier versus applied strain, COHP [35] analysis was conducted. Studies of metallic reactivity have showcased the importance of occupation of antibonding states through the prediction of the d-band center [21,22]. In this case, we use COHP to obtain occupation of bonding and antibonding states with a high number of antibonding states at the Fermi level representing electronic instability. The bonds considered, here, were between each of the O atoms and their nearest P atoms on the lattice [highlighted in Fig. 3(a)]. Selected COHP plots of the transition states at various strains are displayed in Figs. 3(b)–3(e) with negative (positive) representing antibonding (bonding). Starting with the relaxed system [Fig. 3(b)], the green interaction has fewer antibonding states at the Fermi level where the purple interaction does have antibonding occupation at this level. Therefore, this state was electronically unstable, and the system will reconfigure itself via O_2 dissociation. Increasing the applied strain to 3% via zigzag compression with a fixed armchair length [Fig. 3(c)] shows that the transition state remains the same, but the presence of the physisorbed state requires energy to split. If, instead, the compression is applied equibiaxially, then at 1% this original mechanism is maintained with one bond forming first [Fig. 3(d)]. Significantly, the mechanism changes upon increasing strain in this manner to 3% as evidenced through its COHP in Fig. 3(e), and the transition state is different. Here, the bonds form simultaneously as shown through both COHP trends being identical. It was observed that, at this strain, the barrier returns to zero, so this mechanism shift can be attributed as the source for this change. Considering armchair compression with a fixed lateral dimension, COHP analysis indicates that it also undergoes a mechanism change (Fig. S2 of the Supplemental Material [38]). To summarize, when compression is applied in the zigzag direction with pinned lateral dimensions, the barrier increases as the mechanism

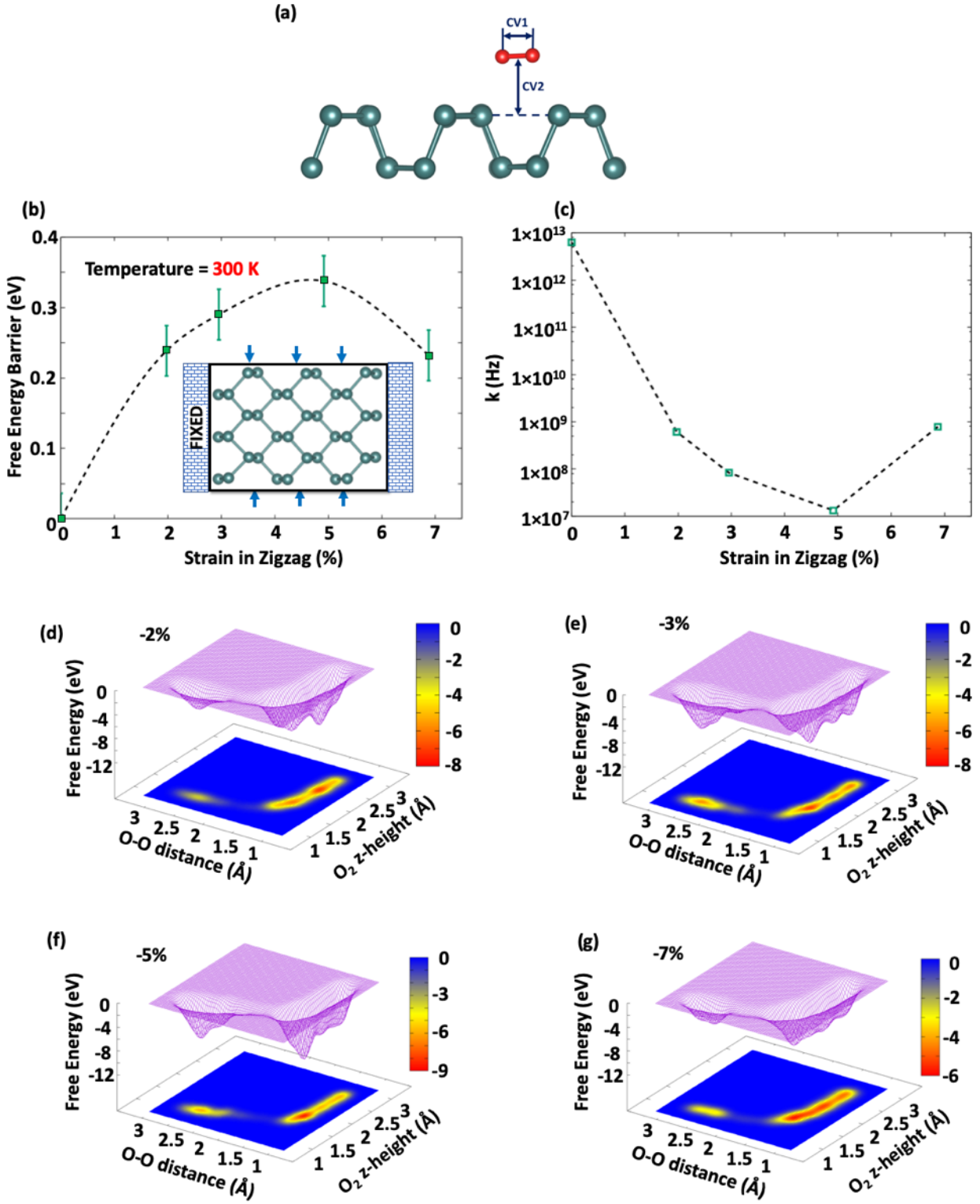

FIG. 4. (a) Illustration of selected collective variables, (b) free-energy barriers at 300 K with boundary condition III, (c) kinetic rate constant as a function of applied strain at 300 K; free-energy landscapes at strains of (d) 2%, (e) 3%, (f) 5%, and (g) 7%.

remains constant. On the other hand, when compression is applied either along the armchair direction with or without a fixed zigzag dimension or equibiaxially, a mechanism shift occurs after 1% allowing spontaneous dissociation. In other words, the lack of mechanism change allows for the system to return to a spontaneous process for the armchair and equibiaxial cases after a critical strain, whereas biaxial zigzag compression does not undergo this shift.

Although these results demonstrate that barriers can be induced at the ground state, they neglect thermal effects. Seeking free-energy barriers, metadynamics biased AIMD simulations were conducted with collective variables illustrated in

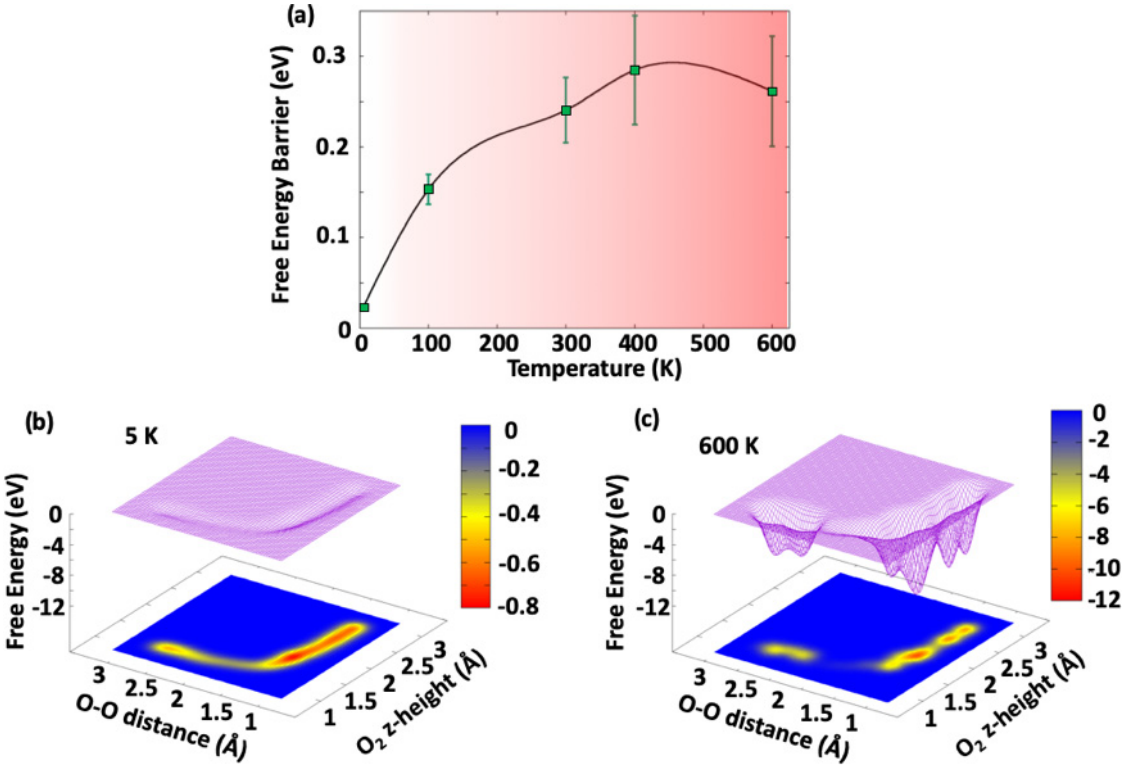

FIG. 5. (a) Energy barriers for fixed lattice parameters as a function of temperature, free-energy landscape for the system with fixed dimensions at (b) 5 K, and (c) 600 K.

Fig. 4(a). Considering the ability of zigzag compression and fixed armchair length strain at introducing a barrier for a range of strains at the ground state, this method of strain will be further examined. Figure 4(b) shows the acquired barriers for this scenario. As strain was introduced, a barrier developed with a peak of 0.33 ± 0.04 eV. However, beyond this point, the barrier begins to decrease, implying that there is a limit to the benefits of compression. Since these runs give free-energy barriers, the Eyring equation may be used to obtain the kinetic rate constant as a function of applied strain [Fig. 4(c)],

$$k = \frac{k_B T}{h} \exp\left(\frac{-G_A}{k_B T}\right),$$

where h is Planck's constant and G_A is the free energy of activation. It is observed that the kinetic rate constant rapidly declines up to five orders of magnitude from 6.5×10^{12} to 1.3×10^{7} Hz. Free-energy landscapes for the corresponding strains are illustrated in Figs. 4(d)–4(g). As the strain increased towards 5%, the physisorbed precursor state becomes deeper in energy like that seen in Fig. 1(c). However, beyond 5%, the well shallows which yields the decrease in activation barrier for this strain. Therefore, in order to minimize the oxidation process at finite temperatures using compression in this manner, the optimal magnitude of applied strain is 5%.

Thermal mismatch where the thermal expansion coefficients differ between the material and the substrate is another method of applying strain to 2D materials which has been successfully used on MoS_2 with dielectric layers as well as polydimethylsiloxane [25] and similarly with WSe_2 [26]. Here, it was simulated by fixing the ground-state lattice parameters and varying the temperature between 5 and 600 K as phosphorene was shown to be unstable at around 673 K [45]. The system stability at each temperature was verified through plotting energy as a function of time (Fig. S3 of the Supplemental Material [38]). To account for the different possible trajectories a system may explore, three independent trials were performed (see Fig. S4 of the Supplemental Material for 400 K [38]). Figure 5(a) shows the free-energy barrier increases as a function of the system temperature where 400 K yielded the maximum barrier of 0.28 ± 0.06 eV. The dip in barrier size shows that there is a limit to the use of strain to increase the barrier. Landscapes for the extremes of the temperature range 5 and 600 K are presented in Figs. 5(b) and 5(c) (see Fig. S6 of the Supplemental Material for the rest [38]). At 5 K, the landscape is flat where, at 100 K and beyond, a physisorbed local minimum emerged creating the barrier to dissociation. Therefore, if phosphorene is deposited on a substrate with a lower coefficient of thermal expansion, then thermal mismatch can induce singlet oxidation resistance.

In conclusion, this Rapid Communication proposes compression to induce oxidation resistance in phosphorene. It was observed that, at the ground state, applying compression can introduce a barrier to singlet O_2 dissociation as large as 0.45 eV thereby decreasing the kinetic rate constant by as much as seven orders of magnitude. COHP analysis indicated a change in the dissociation mechanism thereby explaining the different trends depending on the nature of the compression. To confirm these findings are still valid at finite temperatures, AIMD was used. Fixing the armchair dimension and applying zigzag compression was studied in this manner and demonstrated a maximum induced barrier of 0.33 ± 0.04 eV. This corresponds to a kinetic rate constant as much as five orders

of magnitude less than the relaxed system. Thermal mismatch was also considered and showed an induced barrier reaching as high as 0.28 ± 0.06 eV. Consequently, compressive strain engineering has been identified as a means of increasing the singlet oxidation resistance for phosphorene, opening the door towards future experimental studies.

The authors acknowledge funding by the Natural Sciences and Engineering Research Council of Canada (NSERC) through the Discovery Grant, the Hart Professorship, and the University of Toronto. Compute Canada is also acknowledged for providing computing resources at the SciNet, CalculQuebec, and Westgrid consortia. The authors thank S. Yadav, W. Huxter, and A. Anand for important discussions.

The raw/processed data required to reproduce these findings cannot be shared at this time as the data also form part of an ongoing study.

[1] S. Lin, Y. Li, J. Qian, and S. P. Lau, Mater. Today Energy **12**, 1 (2019).
[2] J. Pang, A. Bachmatiuk, Y. Yin, B. Trzebicka, L. Zhao, L. Fu, R. G. Mendes, T. Gemming, Z. Liu, and M. H. Rummeli, Adv. Energy Mater. **8**, 1702093 (2018).
[3] R. Jain, R. Narayan, S. P. Sasikala, K. E. Lee, H. J. Jung, and S. O. Kim, 2D Mater. **4**, 042006 (2017).
[4] L. Kavalsky, S. Mukherjee, and C. V. Singh, ACS Appl. Mater. Interfaces **11**, 499 (2019).
[5] M. Batmunkh, A. Shrestha, M. Bat-Erdene, M. J. Nine, C. J. Shearer, C. Gibson, A. Slattery, S. Tawfik, M. Ford, S. Dai, S. Qiao, and J. G. Shapter, Angew. Chem., Int. Ed. **57**, 2644 (2018).
[6] W. C. Tan, L. Wang, X. Feng, L. Chen, L. Huang, X. Huang, and K.-W. Ang, Adv. Electron. Mater. **5**, 1800666 (2018).
[7] J. Sun, H. W. Lee, M. Pasta, H. Yuan, G. Zheng, Y. Sun, Y. Li, and Y. Cui, Nat. Nanotechnol. **10**, 980 (2015).
[8] L. Li, L. Chen, S. Mukherjee, J. Gao, H. Sun, Z. Liu, X. Ma, T. Gupta, C. V. Singh, W. Ren, H. M. Cheng, and N. Koratkar, Adv. Mater. **29**, 1602734 (2017).
[9] A. Carvalho, M. Wang, X. Zhu, A. S. Rodin, H. Su, and A. H. Castro Neto, Nat. Rev. Mater. **1**, 16061 (2016).
[10] Q. Li, Q. Zhou, L. Shi, Q. Chen, and J. Wang, J. Mater. Chem. A **7**, 4291 (2019).
[11] X. Wang, Y. Sun, and K. Liu, 2D Mater. **6**, 042001 (2019).
[12] B. Yang, B. Wan, Q. Zhou, Y. Wang, W. Hu, W. Lv, Q. Chen, Z. Zeng, F. Wen, J. Xiang, S. Yuan, J. Wang, B. Zhang, W. Wang, J. Zhang, B. Xu, Z. Zhao, Y. Tian, and Z. Liu, Adv. Mater. **28**, 9408 (2016).
[13] W. Lv, B. Yang, B. Wang, W. Wan, Y. Ge, R. Yang, C. Hao, J. Xiang, B. Zhang, Z. Zeng, and Z. Liu, ACS Appl. Mater. Interfaces **10**, 9663 (2018).
[14] A. Favron, E. Gaufrès, F. Fossard, A. L. Phaneuf-Laheureux, N. Y. W. Tang, P. L. Lévesque, A. Loiseau, R. Leonelli, S. Francoeur, and R. Martel, Nature Mater. **14**, 826 (2015).
[15] A. Ziletti, A. Carvalho, D. K. Campbell, D. F. Coker, and A. H. Castro Neto, Phys. Rev. Lett. **114**, 046801 (2015).
[16] J. Pei, X. Gai, J. Yang, X. Wang, Z. Yu, D. Y. Choi, B. Luther-Davies, and Y. Lu, Nat. Commun. **7**, 10450 (2016).
[17] S. Walia, S. Balendhran, T. Ahmed, M. Singh, C. El-Badawi, M. D. Brennan, P. Weerathunge, M. N. Karim, F. Rahman, A. Rassell, J. Duckworth, R. Ramanathan, G. E. Collis, C. J. Lobo, M. Toth, J. C. Kotsakidis, B. Weber, M. Fuhrer, J. M. Dominguez-Vera, M. J. S. Spencer, I. Aharonovich, S. Sriram, M. Bhaskaran, and V. Bansal, Adv. Mater. **29**, 1700152 (2017).
[18] Y. Abate, D. Akinwande, S. Gamage, H. Wang, M. Snure, N. Poudel, and S. B. Cronin, Adv. Mater. **30**, 1704749 (2018).
[19] C. Elbadawi, R. T. Queralt, Z. Q. Xu, J. Bishop, T. Ahmed, S. Kuriakose, S. Walia, M. Toth, I. Aharonovich, and C. J. Lobo, ACS Appl. Mater. Interfaces **10**, 24327 (2018).
[20] Q. Jiang, J. Zhang, H. Huang, Y. Wu, and Z. Ao, J. Phys. Chem. C **123**, 11591 (2019).
[21] M. Mavrikakis, B. Hammer, and J. K. Nørskov, Phys. Rev. Lett. **81**, 2819 (1998).
[22] Y. Xu, A. V Ruban, and M. Mavrikakis, J. Am. Chem. Soc. **126**, 4717 (2004).
[23] L. A. Kibler, A. M. El-Aziz, R. Hoyer, and D. M. Kolb, Angew. Chem., Int. Ed. **44**, 2080 (2005).
[24] Q. Feng, S. Zhao, D. He, S. Tian, L. Gu, X. Wen, C. Chen, Q. Peng, D. Wang, and Y. Li, J. Am. Chem. Soc. **140**, 2773 (2018).
[25] R. Roldán, A. Castellanos-Gomez, E. Cappelluti, and F. Guinea, J. Phys.: Condens. Matter **27**, 313201 (2015).
[26] G. H. Ahn, M. Amani, H. Rasool, D. H. Lien, J. P. Mastandrea, J. W. Ager, M. Dubey, D. C. Chrzan, A. M. Minor, and A. Javey, Nat. Commun. **8**, 1 (2017).
[27] X. Li, B. Deng, X. Wang, S. Chen, M. Vaisman, S. I. Karato, G. Pan, M. L. Lee, J. Cha, H. Wang, and F. Xia, 2D Mater. **2**, 031002 (2015).
[28] A. J. Mannix, B. Kiraly, M. C. Hersam, and N. P. Guisinger, Nat. Rev. Chem. **1**, 1 (2017).
[29] M. C. Watts, L. Picco, F. S. Russell-Pavier, P. L. Cullen, T. S. Miller, S. P. Bartuś, O. D. Payton, N. T. Skipper, V. Tileli, and C. A. Howard, Nature (London) **568**, 216 (2019).
[30] X. Peng, Q. Wei, and A. Copple, Phys. Rev. B **90**, 085402 (2014).
[31] Z. Yang and G. Liu, Physica B **563**, 72 (2019).
[32] J. Quereda, P. San-Jose, V. Parente, L. Vaquero-Garzon, A. J. Molina-Mendoza, N. Agraït, G. Rubio-Bollinger, F. Guinea, R. Roldán, and A. Castellanos-Gomez, Nano Lett. **16**, 2931 (2016).
[33] L. Vaquero-Garzon, R. Frisenda, and A. Castellanos-Gomez, Nanoscale **11**, 12080 (2019).
[34] J. Gao, G. Zhang, and Y. W. Zhang, Nanoscale **9**, 4219 (2017).
[35] R. Dronskowski and P. E. Blochl, J. Phys. Chem. **97**, 8617 (1993).
[36] V. L. Deringer, A. L. Tchougreeff, and R. Dronskowski, J. Phys. Chem. A **115**, 5461 (2011).
[37] S. Maintz, V. L. Deringer, A. L. Tchougreeff, and R. Dronskowski, J. Comput. Chem. **34**, 2557 (2013).
[38] See Supplemental Material at https://link.aps.org/supplemental/10.1103/PhysRevMaterials.4.021001 for computational details, additional activation barriers and energy profiles, additional COHP plots, thermal stability plots, stochasticity at 400 K,

and additional free-energy landscapes with Refs. [15,35–37,39–41,44,46–59].

[39] P. Giannozzi, S. Baroni, N. Bonini, M. Calandra, R. Car, C. Cavazzoni, D. Ceresoli, G. L. Chiarotti, M. Cococcioni, I. Dabo, A. Dal Corso, S. De Gironcoli, S. Fabris, G. Fratesi, R. Gebauer, U. Gerstmann, C. Gougoussis, A. Kokalj, M. Lazzeri, L. Martin-Samos, N. Marzari, F. Mauri, R. Mazzarello, S. Paolini, A. Pasquarello, L. Paulatto, C. Sbraccia, S. Scandolo, G. Sclauzero, A. P. Seitsonen, A. Smogunov, P. Umari, and R. M. Wentzcovitch, J. Phys.: Condens. Matter **21**, 395502 (2009).

[40] S. Maintz, V. L. Deringer, A. L. Tchougreeff, and R. Dronskowski, J. Comput. Chem. **37**, 1030 (2016).

[41] G. A. Tribello, M. Bonomi, D. Branduardi, C. Camilloni, and G. Bussi, Comput. Phys. Commun. **185**, 604 (2014).

[42] H. Liu, A. T. Neal, Z. Zhu, Z. Luo, X. Xu, D. Tománek, and P. D. Ye, ACS Nano **8**, 4033 (2014).

[43] V. Tran, R. Soklaski, Y. Liang, and L. Yang, Phys. Rev. B **89**, 235319 (2014).

[44] J. P. Perdew, K. Burke, and M. Ernzerhof, Phys. Rev. Lett. **77**, 3865 (1996).

[45] X. Liu, J. D. Wood, K. S. Chen, E. Cho, and M. C. Hersam, J. Phys. Chem. Lett. **6**, 773 (2015).

[46] P. E. Blöchl, Phys. Rev. B **50**, 17953 (1994).

[47] H. Monkhorst and J. Pack, Phys. Rev. B **13**, 5188 (1976).

[48] A. Kokalj, Comput. Mater. Sci. **28**, 155 (2003).

[49] K. Momma and F. Izumi, J. Appl. Crystallogr. **44**, 1272 (2011).

[50] V. Barone, M. Casarin, D. Forrer, M. Pavone, M. Sambi, and A. Vittadini, J. Comput. Chem. **30**, 934 (2009).

[51] H. Jonsson, G. Mills, and K. W. Jacobsen, in *Classical and Quantum Dynamics in Condensed Phase Simulations: Proceedings of the International School of Physics, Lerici, Italy, 1997*, edited by B. J. Berne, G. Ciccotti, and D. F. Coker (World Scientific, Singapore, 1998), p. 385.

[52] B. Sa, Y. L. Li, J. Qi, R. Ahuja, and Z. Sun, J. Phys. Chem. C **118**, 26560 (2014).

[53] H. C. Andersen, J. Chem. Phys. **72**, 2384 (1980).

[54] A. Barducci, G. Bussi, and M. Parrinello, Phys. Rev. Lett. **100**, 020603 (2008).

[55] M. Ghoussoub, S. Yadav, K. K. Ghuman, G. A. Ozin, and C. V. Singh, ACS Catal. **6**, 7109 (2016).

[56] T. Cheng, H. Xiao, and W. A. Goddard, J. Am. Chem. Soc. **138**, 13802 (2016).

[57] K. Klyukin and V. Alexandrov, J. Phys. Chem. C **121**, 10476 (2017).

[58] A. Laio and F. L. Gervasio, Rep. Prog. Phys. **71**, 126601 (2008).

[59] C. F. Bunge, J. A. Barrientos, and A. V. Bunge, At. Data Nucl. Data Tables **53**, 113 (1993).